Table of Contents

Chapter 1

Impurity model

In this chapter, we will consider several models, which describe 1) the case of metallic alloy made of a narrow band element (e.g. transition metal d-band) and non-magnetic element; or a atom absorbed on the surface of a metal; 2) dilute magnetic impurities in metal. These models will promote a widely popular numerical scheme: Dynamical Mean-Field Theory (1992), which has been successfully applied to many strongly-correlated materials.

1.1 Localized state in the continuum

We start by a case with analytic solution:

$$H = E_d d^\dagger d + \sum_k E_k c_k^\dagger c_k + \sum_k V_k (c_k^\dagger d + h.c.) \tag{1.1}$$

where the localized state has a fixed energy E_d, and the conduction band has dispersion E_k. The localized state can be taken as a "impurity" that is embeded in a metal. It contains term in the Hamiltonian includes the mixing between c-electron and d-electron, where the electron can hop to the impurity and the electron can hop off the impurity into the continuum. We first consider the spinless electron in this part first.

Let us define the full Green's function as

$$\hat{G}(\omega+i\eta)=\frac{1}{\omega+i\eta-\hat{H}}$$

$$\sum_{\gamma}\langle\phi_\alpha|(\omega+i\eta-\hat{H})|\phi_\gamma\rangle\langle\phi_\gamma|\hat{G}|\phi_\beta\rangle=\delta_{\alpha\beta}$$

$$\Rightarrow(\omega+i\eta-E_d)G_{dd}-\sum_k V_k G_{k,d}=1 \tag{1.2}$$

$$(\omega+i\eta-E_k)G_{kk}-V_k G_{d,k}=\delta_{k,k'} \tag{1.3}$$

$$(\omega+i\eta-E_k)G_{k,d}-V_k G_{dd}=0 \tag{1.4}$$

$$(\omega+i\eta-E_d)G_{d,k}-V_k G_{k,k}=0 \tag{1.5}$$

Thus we get

$$G_{dd}(\omega)=\frac{1}{\omega+i\eta-E_d-\sum_k\frac{V_k^*V_k}{\omega+i\eta-E_k}}\rightarrow G_{dd}(\omega)=\frac{1}{\omega+i\eta-E_d-\Sigma(\omega)} \tag{1.6}$$

where the self-energy is equal to the hybridization function $\Delta(\omega)\equiv\Sigma(\omega)=\sum_k\frac{V_k^*V_k}{\omega+i\eta-E_k}$. The Green's function has poles at the points where the denominator vanishes, and the poles of Green's function corresponds to excitations of the system: $\tilde{E}_d$, which is the solution of $(\omega-E_d-Re\Sigma(\omega))|_{\omega=\tilde{E}_d}=0$.

Next we can consider a specific example: $E_k=2t\cos k$ which is 1d tight-binding model, and $V_k=V/\sqrt{L}$ with constant coupling strength. The self-energy function is now elementary to evaluate:

$$\Sigma(\omega)=V^2/L\sum_k\frac{1}{\omega-2t\cos k+i\eta}=\frac{V^2}{2\pi}\int_{-\pi}^{\pi}\frac{dk}{\omega-2t\cos k+i\eta}$$

$$\Rightarrow Re\Sigma=\begin{cases}\frac{V^2 sgn(\omega)}{\sqrt{\omega^2-4t^2}},|\omega|>2t\\0,|\omega|<2t\end{cases} \tag{1.7}$$

$$Im\Sigma(\omega)=-\frac{\pi V^2}{2\pi}\int_{-\pi}^{\pi}dk\delta(\omega-2t\cos(k))=\begin{cases}0,|\omega|>2t\\\frac{V^2}{\sqrt{4t^2-\omega^2}},|\omega|<2t\end{cases} \tag{1.8}$$

So the total spectral function is:

$$A(\omega) = \Theta(|\omega| - 2t)[2\pi\delta(\omega - \frac{V^2}{\sqrt{\omega^2 - 4t^2}}) + 2\pi\delta(\omega + \frac{V^2}{\sqrt{\omega^2 - 4t^2}})] + \Theta(2t - |\omega|)\frac{2V^2}{\sqrt{4t^2 - \omega^2}[\omega^2 + \frac{V^4}{4t^2 - \omega^2}]} \tag{1.9}$$

The spectral function shows two separated cases: the pole with $Im\Sigma = 0$, which relates to the bound state; and the pole with $Im\Sigma \neq 0$, which is the resonance state embeded in the continuum. If it is assumed that the bound state occurs ourside of the band, the spectral function has the form $A(\omega) = 2\pi\delta(\omega - E_d - \Sigma) = 2\pi Z\delta(E - \tilde{E}_d)$, with renormalization factor $Z = (1 - \partial\Sigma/\partial\omega)^{-1}|_{\tilde{E}_d}$.

1.2 Anderson impurity model

In history, it has been known that some specific atoms (Fe, Co, Ni) doped in the normal metal has weak magnetism. To interpret this phenomenon, Anderson proposed the following model to describe the formation of local magnetism in alloy (1961)

$$H = \sum_\sigma E_{d\sigma} d_\sigma^\dagger d_\sigma + U n_{d\uparrow} n_{d\downarrow} + \sum_k E_{k\sigma} c_{k\sigma}^\dagger c_{k\sigma} + \sum_{k\sigma} V_k (c_{k\sigma}^\dagger d_\sigma + h.c.) \tag{1.10}$$

The difference between the current case and the last section is, there is an additional interaction term $U n_{d\uparrow} n_{d\downarrow}$, so the model cannot be solved analytically in an exact way. Here we introduce a mean-field decoupling:

$$\begin{aligned} AB &= (\langle A\rangle + \delta A)(\langle B\rangle + \delta B) \approx \langle A\rangle\langle B\rangle + \langle B\rangle\delta A + \langle A\rangle\delta B \\ &= \langle A\rangle\langle B\rangle + \langle B\rangle(A - \langle A\rangle) + \langle A\rangle(B - \langle B\rangle) = \langle B\rangle A + \langle A\rangle B - \langle A\rangle\langle B\rangle \end{aligned} \tag{1.11}$$

And using this relation we get

$$n_{d\uparrow} n_{d\downarrow} \approx \langle n_{d\uparrow}\rangle n_{d\downarrow} + n_{d\uparrow}\langle n_{d\downarrow}\rangle - \langle n_{d\uparrow}\rangle\langle n_{d\downarrow}\rangle \tag{1.12}$$

Then the Hamiltonian will be reduced to

$$\begin{aligned} H &= \sum_{\sigma}(E_{d\sigma} + U\langle n_{d,-\sigma}\rangle)d_{\sigma}^{\dagger}d_{\sigma} + \sum_{k} E_{k\sigma}c_{k\sigma}^{\dagger}c_{k\sigma} + \sum_{k\sigma} V_k(c_{k\sigma}^{\dagger}d_{\sigma} + h.c.) \\ &= \sum_{\sigma} \tilde{E}_{d\sigma}d_{\sigma}^{\dagger}d_{\sigma} + \sum_{k} E_{k\sigma}c_{k\sigma}^{\dagger}c_{k\sigma} + \sum_{k\sigma} V_k(c_{k\sigma}^{\dagger}d_{\sigma} + h.c.) \end{aligned} \tag{1.13}$$

where we define $\tilde{E}_{d\sigma} = E_{d\sigma} + U\langle n_{d,-\sigma}\rangle$.

Then we just define the Green's function as in the last subsection,

$$\hat{G}(\omega + i\eta) = \frac{1}{\omega + i\eta - \hat{H}}$$

$$\sum_{\gamma}\langle\phi_\alpha|(\omega + i\eta - \hat{H})|\phi_\gamma\rangle\langle\phi_\gamma|\hat{G}|\phi_\beta\rangle = \delta_{\alpha\beta}$$

$$\Rightarrow(\omega + i\eta - \tilde{E}_{d\sigma})G_{dd}^{\sigma} - \sum_{k} V_k G_{k,d}^{\sigma} = 1 \tag{1.14}$$

$$(\omega + i\eta - E_k)G_{kk}^{\sigma} - V_k G_{d,k}^{\sigma} = \delta_{k,k'} \tag{1.15}$$

$$(\omega + i\eta - E_k)G_{k,d}^{\sigma} - V_k G_{dd}^{\sigma} = 0 \tag{1.16}$$

$$(\omega + i\eta - \tilde{E}_{d\sigma})G_{d,k}^{\sigma} - V_k G_{k,k}^{\sigma} = 0 \tag{1.17}$$

Thus we get

$$G_{dd}^{\sigma}(\omega) = \frac{1}{\omega + i\eta - \tilde{E}_{d\sigma} - \sum_k \frac{V_k^* V_k}{\omega + i\eta - E_{k\sigma}}} = \frac{1}{\omega + i\eta - \tilde{E}_{d\sigma} - \Sigma^{\sigma}(\omega)} \tag{1.18}$$

$$\Rightarrow \rho_d^{\sigma}(\omega) = -\frac{1}{\pi} Im G_{dd}^{\sigma}(\omega) = \frac{1}{\pi}\frac{Im\Sigma^{\sigma}(\omega)}{(\omega - \tilde{E}_{d\sigma} - Re\Sigma^{\sigma}(\omega))^2 + (Im\Sigma^{\sigma}(\omega))^2} \tag{1.19}$$

Here we assume $\Sigma^{\sigma} = P\sum_k \frac{|V_k|^2}{\omega - E_{k\sigma}} - i\pi\sum_k |V_k|^2\delta(\omega - E_{k\sigma}) \approx i\Delta$ by neglecting frequency dependent real part and assuming the imaginary part is frequent independent. The solution corresponds to a virtual bound state resonance. In this simple approximation, the density of states takes the Lorentzian form.

Then we get the electron number as

$$\langle n_{d\sigma}\rangle = \int_{-\infty}^{E_F} d\omega \rho_d^{\sigma}(\omega) \approx \frac{1}{\pi}\cot^{-1}[\frac{\tilde{E}_{\sigma} - E_F}{\Delta}] \tag{1.20}$$

$(\cot^{-1}(x) = \pi/2 - \arctan(x))$

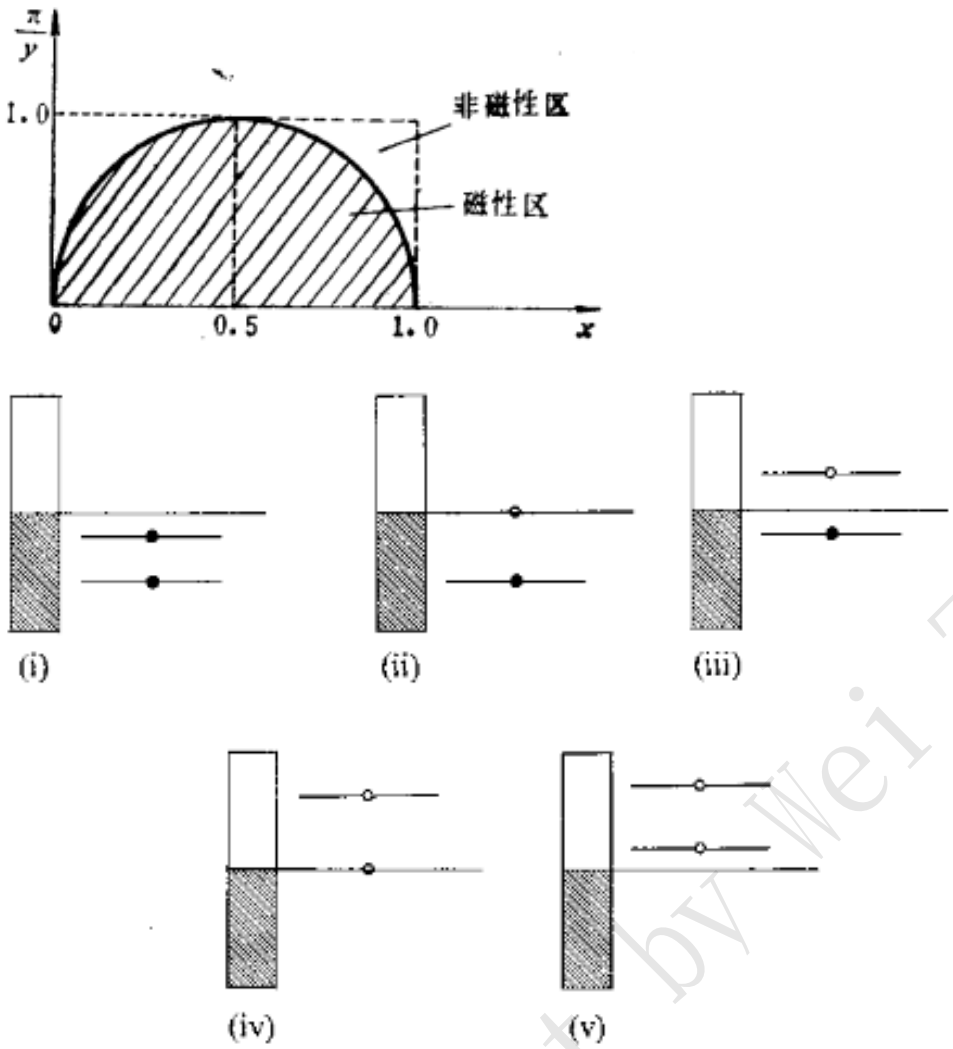

Figure 1.1: Magnetic diagram of Anderson impurity model.

Finally, we construct a self-consistent loop:

$$\langle n_{d\uparrow}\rangle = \frac{1}{\pi}\cot^{-1}\frac{E_d + U\langle n_{d\downarrow}\rangle - E_F}{\Delta} \to \cot(\pi n_\uparrow) = y n_\downarrow - x \tag{1.21}$$

$$\langle n_{d\downarrow}\rangle = \frac{1}{\pi}\cot^{-1}\frac{E_d + U\langle n_{d\uparrow}\rangle - E_F}{\Delta} \to \cot(\pi n_\downarrow) = y n_\uparrow - x \tag{1.22}$$

where $y = U/\Delta$, $x = (E_F - E_d)/\Delta$. For a given x, y, we can solve these two equations and get $n_\uparrow, n_\downarrow$.

The non-magnetic solution $n_\uparrow = n_\downarrow$ always exists, and the equation $\cot \pi n = yn - x$ has only one solution in the regime $0 \le n \le 1$. In addition, there exists the magnetic solution $n_\uparrow \neq n_\downarrow$. The phase diagram is summarized in Fig. 1.2. We see the appearance of magnetic phase is determined by $E_F - E_d$, U and Δ (Hybridization strength).

Next we can try to get some analytical solution. It is convenient to introduce the total occupation $n_d = \langle n_\uparrow \rangle + \langle n_\downarrow \rangle$ and magnetization $m_d = \langle n_\uparrow \rangle - \langle n_\downarrow \rangle$, then the self-consistent equation becomes

$$n_d = \frac{1}{\pi} \sum_{\sigma=\pm} \cot^{-1}[\frac{E_d + U/2(n_d - \sigma m_d)}{\Delta}] \tag{1.23}$$

$$m_d = \frac{1}{\pi} \sum_{\sigma=\pm} \sigma \cot^{-1}[\frac{E_d + U/2(n_d - \sigma m_d)}{\Delta}] \tag{1.24}$$

To find the critical size of interaction strength where a local moment develops, we set the limitation $m_d \to 0$, and obtain:

$$\cot(\pi n_d/2) = \frac{E_d + U_c n_d/2}{\Delta} \tag{1.25}$$

$$1 = \frac{U_c}{\pi\Delta}[\frac{1}{1 + (\frac{E_d + U/2n_d/2}{\Delta})^2}] = \frac{U_c}{\pi\Delta} \sin^2(\frac{\pi n_d}{2}) \tag{1.26}$$

So for the case $n_d = 1$, we have critical strength $U_c = \pi\Delta$. For $U > U_c$ the self-consistent equations have two solutions, corresponding to up and down spin polarization. This is, at half filling of a energy band, the Mott gap opens if the on-site interaction is large enough, the energy level $E_d + U$ becomes empty, and the E_d is fully occupied.

Anderson mean-field theory allows a qualitative understanding of the experimentally observed formation of local moments. When dilute magnetic ions are dissolved in a metal to form a local moment, the condition is the ratio $U/(\pi\Delta)$ is larger than or smaller than 1.

Finally, there are two non-magnetic regimes, one in which the impurity level is predominately in the state with no electrons, i.e. $E_d - E_F > \Delta$, dubbed as empty orbital regime; the other in the state with double occupancy $E_d + U - E_F < \Delta$. These regimes are probably of least interest because the levels are not close enough to the Fermi level for charge fluctuations to be important. Additionally, letting either E_d or $E_d + U$ approach the Fermi level, the charge fluctuations of the impurity become important. This regime know as the intermediate valence regime, which cannot be described by the simple Anderson impurity model.

1.3 Dynamical mean field theory

In the last section, we discuss a numerical method, dynamical mean-field theory, to treat strongly-correlated materials. The dynamical mean-field theory has deep relation with the Kondo impurity problem as shown above (so I put it in this chapter). In principle, dynamical mean-field theory is designed to treat systems with local effective interactions that are strong compared with the independent-particle terms that lead to delocalized band-like states. Interactions are taken into account by a many-body calculation for an auxiliary system, a site embedded in a dynamical mean field, that is chosen to best represent the coupling to the rest of the crystal. This section is devoted to the general formulation, the single-site approximation where the calculation of the self-energy is mapped onto a self-consistent quantum impurity problem, and instructive examples for the Hubbard model on a Bethe lattice.

The topic of this section is dynamical mean-field theory, which is also a Greens function method in which the key quantity is the self-energy. It is designed to treat strong interactions for electrons in localized atomic-like states, such as the d and f states in transition metals, lanthanide and actinide elements and compounds. Instead of a systematic perturbation expansion, the methods are constructed to be correct in three limits: isolated atoms including all effects of interactions, an extended solid with no interactions, and the limit of infinite dimensions where mean-field theory is exact. DMFT is designed to treat materials with local moments in a disordered phase, e.g., a magnetic material such as Ni and NiO above the transition temperature; metalinsulator transitions, such as in V_2O_3; and highly renormalized behavior, such as in the heavy fermion material $CeIrIn_5$, where quasi-particles emerge at low temperature with mass 100 times that expected in an independent-particle picture.

The problem we faced is the lattice Hubbard model described by the Hamiltonian:

$$H = \sum_{ij\sigma}[t_{ij,\sigma}c^{+}_{i\sigma}c_{j\sigma} + h.c.] + (\varepsilon_0 - \mu)\sum_i n_{i\sigma} + U\sum_i n_{i,\uparrow}n_{i,\downarrow}. \tag{1.27}$$

Unfortunately, this model can not be solved exactly so far. People have developed many different approximated method to solve it. One of the physical intuition is to map the Hubbard model to the local quantity coupled to an effective bath (the rest of the lattice), as shown in Fig. 1.2. It is valuable to point out the overall strategy to utilize auxiliary systems (bath). The advantages of an auxiliary system are that in principle it can reproduce selected properties of

the full interacting many-body system by calculations on a simpler system; in practice it can provide avenues for useful approximations.

An essential part of the strategy is that the auxiliary embedded system must be soluble for a range of possible baths and it must be flexible enough to describe the chosen properties of the actual system. In principle, it may be possible to find a bath that reproduces exactly some selected property of the small system. In general, however, one must make approximations based on physical arguments to find a criterion for the auxiliary system that best represents the actual system.

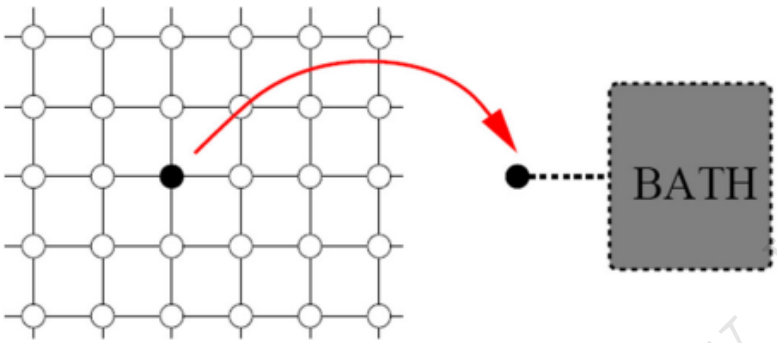

Figure 1.2: Schematic illustration of an auxiliary embedded system: Mapping a lattice problem to an impurity model. The black circle represents a part of the actual system (with full interactions), which is small enough that the interacting electron problem can be solved. The shaded region represents the bath, an effective (and non-interacting) medium that is simplified enough that the desired properties can be calculated. Coupling with the bath can take various forms, for example, the arrows represent electrons hopping to and from the bath at different times that can be described by a hybridization function $\Delta(\omega)$. By construction, the auxiliary embedded system can be solved with no approximation; the approximations enter in the way it is used to represent the actual system of interacting electrons.

The representative site is described by effective Anderson impurity model:

$$
\begin{aligned}
H_{AIM} &= H_{coupling} + H_{site} + H_{bath}, \qquad (1.28)\\
H_{site} &= U n_{i,\uparrow} n_{i,\downarrow} + (\varepsilon_0 - \mu)(n_{i\uparrow} + n_{i\downarrow}),\\
H_{bath} &= \sum_{l,l',\sigma} a^{+}_{l\sigma} a_{l'\sigma} + h.c. = \sum_{k\sigma} \varepsilon_k a^{+}_{k\sigma} a_{k\sigma},\\
H_{couping} &= \sum_{l,i,\sigma} V_{l,i} (a^{+}_{l\sigma} c_{i\sigma} + h.c.)
\end{aligned}
$$

where $a_{l\sigma}$ describes the fermion belong to the bath or environment. For the present discussion we assume interactions are confined to each site and the only coupling between sites in the hamiltonian is independent-particle hopping indicated by the lines connecting the sites in the

figure. To keep the notation simple, we describe the theory in terms of sites in the crystal, with the understanding that the same formulas apply whether the site is a single atom or a cell of atoms.

At the first step, the electron hopping on/off the impurity is thus described by the bath Green's function:

$$G_0(i\omega) = \frac{1}{i\omega_n + \mu - \varepsilon_0 - \Delta(i\omega_n)} \tag{1.29}$$

where $\Delta = \sum_k \frac{|V_{i,k}|^2}{i\omega_n - \varepsilon_k}$ is the hybridzaition function (See discussion in Sec. B Anderson impurity model). Here we effectively think about $U = 0$ case, and the solution above is analog to non-interacting Green's function.

And the interaction term defines an effective Anderson impurity problem for a single correlated atom. Solution of this quantum impurity problem gives one the local Greens function G_{imp}, which is the full Green's function at the impurity site for Eq. 1.28. We just leave the problem "how to solve impurity model" in next section later. Supposed that we can obtain G_{imp}, we define the local self-energy $\Sigma_{imp}(i\omega_n)$ as

$$\Sigma_{imp}(i\omega_n) = G_0^{-1}(i\omega_n) - G_{imp}^{-1}(i\omega_n) \tag{1.30}$$

Second, we define lattice Green's function as G_{latt} as (Or, the theory is cast in terms of the single-particle Greens function for the crystal)

$$G_{latt}(k, i\omega_n) = \frac{1}{i\omega_n + \mu - \varepsilon_0 - \varepsilon_k - \Sigma(k, i\omega_n)} \tag{1.31}$$

The independent-particle bands are given by ε_k and effects of interactions are included in the self-energy $\Sigma(k, i\omega_n)$. Here we can think about G_{latt} as the full Green's function of the original Hubbard model Eq 1.27.

The goal is to provide useful methods to calculate the self-energy, and the strategy in DMFT is to utilize an array of auxiliary systems on the sites of the crystal. The only role for the auxiliary system is to provide a way to determine the self-energy and the only results needed from the calculation for the auxiliary system are the Greens function. In DMFT, we introduce

the key mean-field approximation:

$$\Sigma(k, i\omega_n) \approx \Sigma_{imp}(i\omega_n). \tag{1.32}$$

i.e. the self-energy is purely local. This approximation tells us that, the Green's function of lattice Hubbard model is translational invariant, and each site self-energy coincides with that of the mapped impurity model. That is, DMFT assumes that the local correlations are largest and the longer-range correlations are weaker and are approximated in practical methods.

Then we further define the local Green's function as

$$G_{loc}(i\omega_n) = \sum_k G_{latt}(k, i\omega_n) \tag{1.33}$$

where the sum is over the whole BZ.

Finally, one obtains the DMFT self-consistency condition:

$$G_{loc}(i\omega_n) = G_{imp}. \tag{1.34}$$

Using Eq.1.29, 1.30, we get the alternative form for self-consistent condition:

$$\begin{aligned} G_{loc}(i\omega_n) &= \sum_k \frac{1}{i\omega_n + \mu - \epsilon_0 - \epsilon_k - \Sigma(k, i\omega_n)} \\ &= \sum_k \frac{1}{G_0^{-1}(i\omega_n) + \Delta(i\omega_n) - \epsilon_k - \Sigma(i\omega_n)} \\ &= \sum_k \frac{1}{\Delta(i\omega_n) + G_{loc}^{-1}(i\omega_n) - \varepsilon_k} \end{aligned} \tag{1.35}$$

The above precedure is similar to the Wess mean-field, and we list a comparison in the Table.

1.3.1 Numerical loop

In practice, the self-consistent loop contains the following steps:

1. Start with a guess for $\Sigma(k, i\omega_n)$ (typically, $\Sigma(k, i\omega_n) = 0$);

2. Make the DMFT approximation: $\Sigma(k, i\omega_n) \approx \Sigma_{\text{imp}}(i\omega_n)$;

Ising	Hubbard
$H = -J\sum_{\langle ij\rangle}\sigma_i\sigma_j$	$H = -\sum_{\langle ij\rangle} t_{ij}c^\dagger_{i\sigma}c_{i\sigma} + \sum_i U n_{i\uparrow}n_{i\downarrow}$
$H_{\text{eff}} = -Jh_{\text{eff}}\sigma$ $m = \langle\sigma\rangle$	$S_{\text{eff}} = -\int_0^\beta c^\dagger_\sigma(\tau)\mathcal{G}^{-1}_\sigma(\tau-\tau')c_\sigma(\tau') + \int_0^\beta d\tau\, U n_\uparrow(\tau)n_\downarrow(\tau)$ $G_{\sigma\text{imp}}(\tau) \equiv -\left\langle Tc_\sigma(\tau)c^\dagger_\sigma(0)\right\rangle_{S_{\text{eff}}}$
$h_{\text{eff}} = zJm$	$\Sigma_{\sigma\text{imp}}[\mathcal{G}](i\omega_n) \equiv \mathcal{G}^{-1}_\sigma(i\omega_n) - G^{-1}_{\sigma\text{imp}}[\mathcal{G}](i\omega_n)$ $G_{\sigma\text{imp}}[\mathcal{G}](i\omega_n) = \sum_k \frac{1}{i\omega_n + \mu - \epsilon_k - \Sigma_{\sigma\text{imp}}[\mathcal{G}](i\omega_n)}$

Figure 1.3: Compare the mean-field with dynamical mean-field theory.

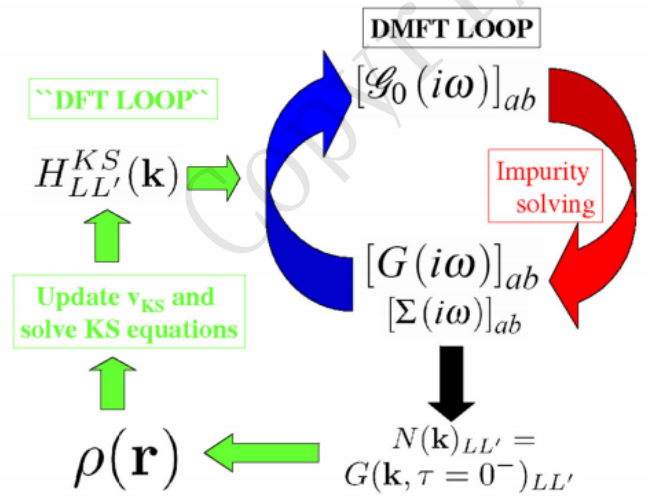

Figure 1.4: Schmatical plot for DMFT loop.

3. Compute the local Green's function $G_{\mathrm{loc}}(i\omega_n)$;

4. Compute the dynamical mean field (Eq. 1.30,1.29) $\Delta(\omega) = i\omega_n + \mu - G_{loc}^{-1}(i\omega_n) - \Sigma_{imp}(i\omega_n)$, and then construct bath accordingly;

5. Solve the AIM for a new impurity Green's function $G_{\mathrm{imp}}(i\omega_n)$, extract its self-energy: $\Sigma_{imp}(i\omega_n) = G_0^{-1}(i\omega_n) - G_{imp}^{-1}(i\omega)$;

6. Go back to step 2 until convergence, namely when $G_{imp}^{n}(i\omega_n) \approx G_{imp}^{n+1}(i\omega_n)$.

This is also shown in the Figure 1.4. Please note that, in the real material calculation, we can also get G_{latt} by DFT.

1.3.2 Impurity solver

The key step in DMFT is step 5: to solve the Anderson impurity problem. This step costs most of computational time. One can solve this Anderson impurity problem using approximation method, or numerically exact method. If it is treated in other approximation method, the correlation effect doesnot include correctly. Thus, we prefer the unbiased way.

Solving the Anderson impurity model amounts to computing observables such as the interacting Green's function and related spectral function for a given hybridization function. There exists a number of ways to solve the Anderson impurity model, including exact diagonalization, the numerical renormalization group, iterative perturbation theory, the Hirsch-Fye and continuous-time quantum Monte Carlo methods. Although the above impurity solvers have been proposed and developed for decades, they have strength and weakness. For instance, the numerical renormalization group, being designed for impurity problems, is unable to resolve a good resolution of spectral density at high energy regime, due to the limitation of logarithmic discretization of the bath density of states. Moreover, related generalization of numerical renormalization group to the multiorbital or multi-band lattice model is still unfeasible. Quantum Monte Carlo method can efficiently deal with multi-band models, but it lacks high resolution of the spectral function when formulated in imaginary time, due to the ill-conditioned analytic continuation from imaginary to real frequencies. Exact diagonalization naturally works with real frequencies, but it is severely limited by its accessible system sizes. This again reduces the spectral resolution considerably.

On the other hand, over more than twenty years of the development, DMRG has become a mature numerical technique dealing with generalized Hamiltonian, which is widely accepted as the most successful method for one-dimensional interacting systems. Since the impurity problem in DMFT can be transformed to be actually one-dimensional, it is natural to use DMRG as an impurity solver in DMFT numerical loop. Actually, the existing works demonstrate that DMRG is able to give very accurate solution for impurity model.

In some ways, DMFT is analogous to the KohnSham method but it involves a dynamic Greens function and self-energy instead of the static density and the exchangecorrelation potential.

1.3.3 DMFT self-consistent condition on the Bethe lattice

In this section, we briefly discuss the self-consistent condition, hybridization function for the Bethe lattice, with or without magnetic field. The Bethe lattice is interesting due to its specific form of density of states (DOS), which can simplify the DMFT self-consistent condition. It enables us not to use any other feature from the Bethe lattice other than the DOS form.

On the Bethe lattice, the single-particle DOS (in the absence of interaction term) takes a semi-elliptic form:

$$\rho^0(\omega) = -\frac{1}{\pi} ImG^0(\omega) = \frac{2}{\pi D^2}\sqrt{D^2 - \omega^2}, \tag{1.36}$$

where $2D$ stands for the band width of system and the bare lattice Green's function $G^0(\omega)$ takes a particularly simple continued fraction representation with constant coefficients

$$G^0(\omega) = \cfrac{1}{\omega - \cfrac{\frac{D^2}{4}}{\omega - \cfrac{\frac{D^2}{4}}{\omega - \cdots}}}. \tag{1.37}$$

With the help of the Dyson equation, the full lattice Green's function $G(\omega)$ can be expressed to be

$$\frac{1}{G(\omega)} = \frac{1}{G^0(\omega - \Sigma(\omega))} = \omega - \Sigma(\omega) - \cfrac{\frac{D^2}{4}}{\omega - \Sigma - \cfrac{\frac{D^2}{4}}{\omega - \Sigma - \cfrac{\frac{D^2}{4}}{\omega - \Sigma \cdots}}} = \omega - \Sigma(\omega) - \left(\frac{D^2}{4}\right) G(\omega), \tag{1.38}$$

where $\Sigma(\omega)$ is the self-energy function. Importantly, several remarks are in order. First, we have assumed that self-energy function $\Sigma(\omega)$ is uniform in real-space thus it is independent of momentum quantum number, which is one key assumption of DMFT. Due to this assumption, self-energy function behaves as a global energy shift to frequency ω. Last but not least, the continued fraction does not change when it is evaluated at a deeper level because its coefficients are constant.

On the other hand, we can write the bare Green's function of the Anderson impurity model $g^0(\omega)$ with the help of the so-called hybridization function $\Gamma(\omega)$ as

$$g^0(\omega) = \frac{1}{\omega - \Gamma(\omega)} \tag{1.39}$$

where the continued fraction of $\Gamma(\omega)$ is

$$\Gamma(\omega) = \cfrac{V^2}{\omega - \varepsilon_0 - \cfrac{\gamma_0^2}{\omega - \varepsilon_1 - \cfrac{\gamma_1^2}{\omega - \cdots}}}. \tag{1.40}$$

For an infinite homogeneous system we have $\gamma_i = D/2$, $\varepsilon_i = 0$ and $V = D/2$. From the Dyson equation, the impurity Green's function of Anderson impurity model reads

$$\frac{1}{g(\omega)} = \frac{1}{g^0(\omega)} - \Sigma(\omega) = \omega - \Sigma(\omega) - \Gamma(\omega). \tag{1.41}$$

Based on the self-consistency condition, we set Eqs. (1.38,1.41) equal and obtain the simpler self-consistency condition:

$$\Gamma(\omega) = \frac{D^2}{4} G(\omega). \tag{1.42}$$

This equation is simple and it provides a direct way to compute the hybridization function $\Gamma(\omega)$ (Eq. (1.40)) of the next iteration of the Anderson impurity model from the lattice propagator $G(\omega)$.

At last, we solve a single-orbital Hubbard model on the Bethe lattice in the absence of magnetic field, which is given by the Hamiltonian

$$\mathcal{H} = U \sum_i \left(n_{i,\uparrow} - \frac{1}{2} \right) \left(n_{i,\downarrow} - \frac{1}{2} \right) - t \sum_{\langle i,j \rangle, \sigma} c_{i,\sigma}^\dagger c_{j,\sigma} \tag{1.43}$$

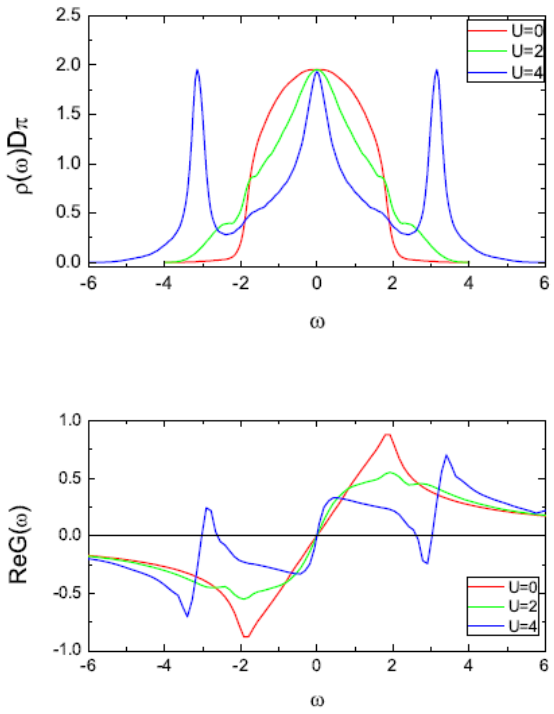

Figure 1.5: Dynamical DMRG solution for one dimensional single-impurity Anderson model (by setting $V = D/2$, $\gamma_i = \gamma = 1.0$ in Eq. 1.40) for different interaction strength $U = 0, D, 2D$: (Left) Spectral densities (imaginary part of Green function by scaling a global constant πD) and (Right) Real part of Green functions as a function frequency ω. For DMRG simulation, we choose a chain length $L = 80$ fermionic sites (after mapping into two-component spinless model, we have $L' = 160$ lattice sites). We kept 128 states in each DMRG block and the resulting projection error is less than 10^{-10}. In the dynamical DMRG calculation, we use a smearing energy $\eta = 0.1D$ before deconvolution calculation.

where $c^\dagger_{i,\sigma}$ creates one electron with spin$-\sigma$ at site i and $n_{i,\sigma}$ is occupation operator. The basic physics of the hubbard model comes from the competition between the local repulsive interaction and kinetic term consisting of hopping from one site to the other site. The interaction is diagonal in real space and hence tends to make the electrons local in real space, while the kinetic energy is diagonal in momentum space and hence tends to make the electrons extended in real space. So the interaction favors an insulating phase, whereas the kinetic energy favors a metallic phase, depending on the relative strength of U/t.

Here we solve the Hubbard Hamiltonian, with DMFT scheme. The related key DMFT self-consistent condition has been discussed in Sec. 1.3.3. Fig. 1.6 shows our results for various interaction strength U in the metallic phase ($U < U_c \approx 2.6D$). Here we choose the one-dimensional impurity model enclosing $L = 80$ fermionic sites, which is solved by DMRG algorithm by limiting each DMRG block with dimension $M = 128$. The obtained projection error in DMRG calculation are all negligible small (less than 10^{-10}), indicating good convergence of DMRG output

from core impurity model. As to computational performance, by setting parameter $U = 2D$, the typical (physical) time cost is 63 minutes for each DMFT loop (on two 3.90GHz cores). Here we set the simulation parameter as the broadening energy $\eta = 0.1D$ and frequency scan step $\Delta\omega = \eta$ ($\omega \in [-6.0, 6.0]$), and use the mixed Bath discretization.

The obtained spectral densities faithfully recover the previous DMFT+DMRG calculations, with key features including the pinning criterion $\rho(\omega = 0) = \frac{2}{\pi D}$ for all interaction strength, and the side peaks at the inner edges of Hubbard bands in strong interaction regime ($U = 2D$). Compared with previous numerical renormalization group calculations, current DMFT+DMRG scheme deal with low frequency and high frequency with the equal weight, thus we can get correct both Kondo resonance peak in the low frequency and Hubbard satellite bands (non-coherent peak) in the high frequency. Compared with the Chebyshev-based simulations, current DMFT+DMRG reaches a better convergence. In a word, under DMFT+DMRG scheme, by using the two-component mapping, a better convergence and computational performance is available.

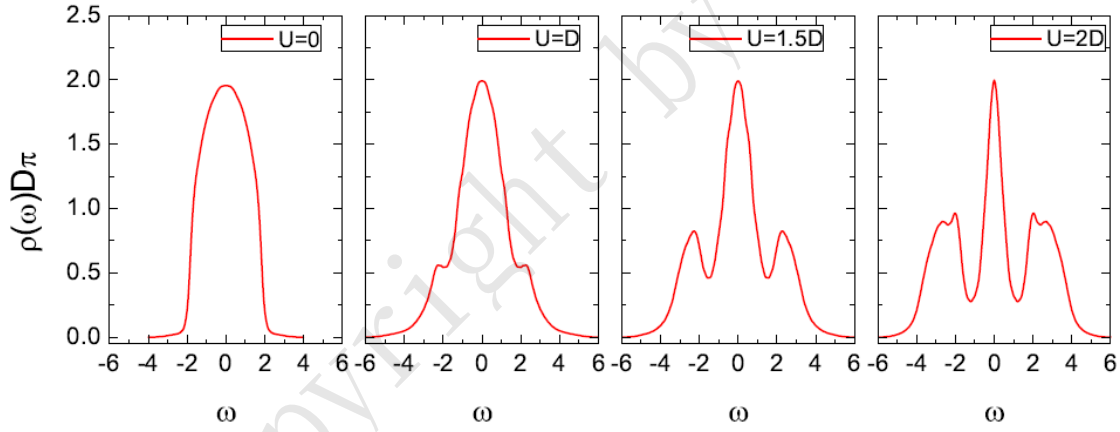

Figure 1.6: Spectral densities of single-orbital Hubbard model on the Bethe lattice obtained by DMFT scheme. We choose the impurity model enclosing $L = 80$ fermionic sites, which is solved by DMRG algorithm by limiting each DMRG block with dimension $M = 128$. Before the deconvolution calculation, we select the broadening parameter as $\eta = 0.1D$.

1.3.4 Electronic correlations in materials: LDA+DMFT

Until recently the electronic properties of solids were investigated by two essentially separate communities, one using model Hamiltonians in conjunction with many-body techniques, the other employing density functional theory (DFT). DFT and its local density approximation (LDA) have the advantage of being ab initio approaches which do not require empirical parameters as

input. Indeed, they are highly successful techniques for the calculation of the electronic structure of real materials. However, in practice DFT/LDA is seriously restricted in its ability to describe strongly correlated materials where the on-site Coulomb interaction is comparable with the band width. Here, the model Hamiltonian approach is more powerful since there exist systematic theoretical techniques to investigate the many-electron problem with increasing accuracy. The two approaches are therefore complementary. In view of the individual power of DFT/LDA and the model Hamiltonian approach, respectively, a combination of these techniques for ab initio investigations of correlated materials including, for example, f-electron systems and Mott insulators, would be highly desirable.

The recently developed LDA+DMFT method, a new computational scheme which merges electronic band structure calculations and the DMFT. Starting from conventional band structure calculations in the LDA the correlations are taken into account by the Hubbard interaction and a Hunds rule coupling term. The resulting DMFT equations are solved numerically, e.g., with a quantum Monte-Carlo (QMC) algorithm. By construction, LDA+DMFT includes the correct quasiparticle physics and the corresponding energetics (in some showcases). It also reproduces the LDA results in the limit of weak Coulomb interaction U. More importantly, LDA+DMFT correctly describes the correlation induced dynamics near a Mott-Hubbard MIT and beyond. Thus, LDA+DMFT is able to account for the physics at all values of the Coulomb interaction and doping level.

1.4 Numerical Renormalization Group

Particular attention has been devoted to the effect of strong electron-electron interactions (also referred to as "strong correlation effects") in the transport properties of nanodevices. Electrons can now be confined and manipulated in a controllable way in semiconductor quantum dots, scanning tunneling microscopy set-ups and molecular junctions, allowing for a myriad of single-particle and many-body effects to be probed in detail. Prominent among these is the Kondo effect, arising from the screening of a local magnetic moment (such as a single electron spin) by the surrounding electrons in a continuum, forming a many-body bound state. The essential physics of the Kondo effect in equilibrium is captured by quantum impurity models describing a magnetic impurity coupled to Fermi reservoirs, such as the Kondo model or, more generally, the Anderson model. The formulation of the latter includes charge fluctuations, thus allowing for the

description of equilibrium transport properties through the impurity. One of the most accurate schemes for obtaining the low-energy excitation spectra in these and other quantum impurity models is given by Kenneth Wilson's Numerical Renormalization Group (NRG) method.

The non-perturbative nature of this method allows the calculation of physical properties (such as spectral functions and magnetization curves) at arbitrarily low temperatures and excitation energies, precisely in the region where the Kondo effect is fully developed. In this sense, the NRG method constitutes a very powerful tool to explore different effects in transport properties of strongly correlated systems. In particular, there has been a large interest on the use of NRG for equilibrium transport calculations in quantum dot systems.

The NRG method is special designed for quantum impurity systems, with a small impurity an object with a small number of degrees of freedom with arbitrary interactions coupled to a non-interacting bath usually a free conduction band, that is non-interacting fermions. Nevertheless, there is an enormous range of physical phenomena which can be realized in such systems, and to which the NRG can be applied.

In these lecture notes, we will purely focus on the single-impurity Anderson model. The Hamiltonian of a general quantum impurity model consists of three parts, the impurity H_{imp}, the bath H_{bath}, and the coupling between impurity and bath,:

$$H = H_{imp} + H_{bath} + H_{imp-bath} \tag{1.44}$$

In the single-impurity Anderson model (siAm), the impurity consists of a single level with energy E_d. The Coulomb repulsion between two electrons occupying this level (which then must have opposite spin) is given by U:

$$H_{imp} = \sum_{\sigma} E_d d_{\sigma}^{\dagger} d_{\sigma} + U d_{\uparrow}^{\dagger} d_{\uparrow} d_{\downarrow}^{\dagger} d_{\downarrow} \tag{1.45}$$

with d_σ ($d_\sigma^\dagger$) annihilation (creation) operators for a fermion with spin$-\sigma$ on the impurity level.

The bath could be 1D, 2D, or 3D electron band.

$$H_{bath} = \sum_{k,\sigma} \epsilon_k c_{k,\sigma}^{\dagger} c_{k,\sigma} \tag{1.46}$$

The impurity and bath coupling term describes

$$H_{imp-bath} = \sum_{k,\sigma} V_k (d_\sigma^\dagger c_{k,\sigma} + h.c.) \tag{1.47}$$

We can now easily calculate the form of the hybridization function using equations of motion. The essential point is that the one-particle Green function $G(z) = \langle d^\dagger d \rangle$ can be written in the form

$$G(z) = \frac{1}{z - E_d - \Delta(z) - \Sigma(z)} \tag{1.48}$$

where $\Sigma(z)$ is the correlation part from on-site interaction, and the hybridization function is

$$\Delta(z) = \sum_k \frac{V_k^2}{z - \epsilon_k} \tag{1.49}$$

Usually it is the imaginary part of this quantity which is referred to as the hybridization function:

$$\Delta(\omega) = -\lim_{\eta \to 0} \Im \Delta(z = \omega + i\eta) = \pi \sum_k V_k^2 \delta(\omega - \epsilon_k) \tag{1.50}$$

1.4.1 Logarithmic discretization

The Anderson model is

$$\mathcal{H} = E_d d^\dagger d + \sum_k \epsilon_k c_k^\dagger c_k + \sum_k V_k (d^\dagger c_k + d c_k^\dagger) \tag{1.51}$$

The influence of the bath on the impurity is completely determined by the so-called hybridization function $\Delta(\omega)$. Thus, if we are only interested in the impurity contributions to the physics of the SIAM, we can rewrite the Hamiltonian in a variety of ways, provided the manipulations involved do not change the form of $\Delta(\omega)$. Next, we use continuous energy representation form

$$H = E_d d^\dagger d + \int_{-1}^{1} d\epsilon g(\epsilon) c_\epsilon^\dagger c_\epsilon + \int_{-1}^{1} h(\epsilon)(d^\dagger c_\epsilon + d c_\epsilon^\dagger) \tag{1.52}$$

To understand it, one needs the relation between sum up in momentum and sum up in energy

space: $\int dk = \int \rho(E)dE$. Here we renormalize the energy ranging in $[-1.1]$. The conduction band is now assumed to be continuous, with the band operators satisfying the standard fermionic commutation relations: $\{a_\epsilon^\dagger, a_{\epsilon'}\} = \delta_{\epsilon,\epsilon'}$.

Please note that function $g(\epsilon)$ and $h(\epsilon)$ are not independent. In fact, they are related by the hybridization function:

$$\Delta(\omega) = \pi \sum_k V_k^2 \delta(\omega - \epsilon_k) \tag{1.53}$$

$$= \pi \int_{-1}^{1} d\epsilon h^2(\epsilon)\delta(\omega - g(\epsilon)) \tag{1.54}$$

$$= \pi h^2(g^{-1}(\omega))\frac{d}{d\omega}g^{-1}(\omega) \tag{1.55}$$

where we use the relationship $\delta[f(x)] = \frac{\delta(x-x_i)}{|f'(x_i)|}$, and x_i is the root of $f(x)$. $g^{-1}(\omega)$ is the inverse function of $g(\omega)$: $g^{-1}(g(\omega)) = \omega$. For a constant $\Delta(\omega) = \Delta_0$ within the interval $[-1, 1]$, we have $g^{-1}(\omega) = \omega$ (this corresponds to $g(\epsilon) = \epsilon$) and $h^2(\epsilon) = \Delta_0/\pi$.

To access low energy physics, the NRG algorithm adopts the logarithmic discretization scheme. According to such a scheme, the band interval $[-1, 1]$ is divided into intervals $[-\Lambda^{-n}, -\Lambda^{-(n+1)}]$ and $[\Lambda^{-(n+1)}, \Lambda^{-n}]$ (n=0,1,2,...), where parameter $\Lambda > 1$. Thus, each interval width is $d_n = \Lambda^{-n}(1 - \Lambda^{-1})$. For each interval, we introduce a complete set of orthonormal functions

$$\psi_{np}^{\pm}(\epsilon) = \begin{array}{c} \frac{1}{\sqrt{d_n}} e^{\pm i\omega_n p\epsilon}, \Lambda^{-(n+1)} < \epsilon < \Lambda^{-n} \\ 0, outside this interval. \end{array} \tag{1.56}$$

The index p takes all integer values between $-\infty$ and ∞, and the fundamental frequencies for each interval are given by $\omega_n = 2\pi/d_n$.

In this new basis, the original conduction electron operators can be expanded as

$$\hat{c}_\epsilon = \sum_{np} \hat{a}_{np}\psi_{np}^{+}(\epsilon) + \hat{b}_{np}\psi_{np}^{-}(\epsilon) \tag{1.57}$$

$$\hat{a}_{np} = \int_{-1}^{1} d\epsilon [\psi_{np}^{+}(\epsilon)]^* c_\epsilon \tag{1.58}$$

$$\hat{b}_{np} = \int_{-1}^{1} d\epsilon [\psi_{np}^{-}(\epsilon)]^* c_\epsilon \tag{1.59}$$

The operators $\hat{a}_{np}$ and $\hat{b}_{np}$ form another complete set of independent and discrete electron oper-

ators obeying the normal anti-commuting relations

$$\{a_{np}, a^{\dagger}_{n',p'}\} = \delta_{n,n'}\delta_{p,p'} \tag{1.60}$$

The Hamiltonian is now expressed in terms of these discrete operators. In particular, the transformed hybridization term (first part only) is

$$\int_{-1}^{1} d\epsilon h(\epsilon) d^{\dagger} c_{\epsilon} = d^{\dagger} \sum_{np} [a_{np} \int^{+,n} d\epsilon h(\epsilon) \psi^{+}_{np}(\epsilon) + b_{np} \int^{-,n} d\epsilon h(\epsilon) \psi^{-}_{np}(\epsilon)] \tag{1.61}$$

For a constant $h(\epsilon) = h$, the integral filter out the $p = 0$ component only

$$\int^{+,n} d\epsilon h \psi^{\pm}_{np}(\epsilon) = \sqrt{d_n} h \delta_{p,0} \tag{1.62}$$

In other words, the impurity couples only to the $p = 0$ components of the conduction band states. It will become clear soon, that this point was essential in Wilsons original line of arguments, so we would like to maintain this feature ($h(x)$ being constant in each interval of the logarithmic discretization) also for a general, non-constant $\Delta(\omega)$. Thus we simplify the version of transformation formula as

$$\psi^{\pm}_{n,p=0}(\epsilon) = \begin{matrix} \frac{1}{\sqrt{d_n}}, \Lambda^{-(n+1)} < \epsilon < \Lambda^{-n} \\ 0, outside this interval. \end{matrix} \tag{1.63}$$

and

$$c_{\epsilon} = \sum_{np} a_{np} \psi^{\dagger}_{n,p=0}(\epsilon) + b_{np} \psi^{-}_{n,p=0}(\epsilon) \tag{1.64}$$

$$a_{n,p=0} = \frac{1}{\sqrt{d_n}} \int^{+} d\epsilon c_{\epsilon}, \int^{+} d\epsilon = \int_{x_{n+1}}^{x_n} d\epsilon \tag{1.65}$$

$$b_{n,p=0} = \frac{1}{\sqrt{d_n}} \int^{-} d\epsilon c_{\epsilon}, \int^{-} d\epsilon = \int_{-x_n}^{-x_{n+1}} d\epsilon \tag{1.66}$$

Moreover, we can also set a step function for h (but keeping the definition of $\psi^{\pm}$):

$$h(\epsilon) = h^{\pm}_n, \Lambda^{-(n+1)} < \pm\epsilon < \Lambda^{-n} \tag{1.67}$$

$$(h^{\pm}_n)^2 = \frac{1}{d_n \pi} \int^{\pm} d\epsilon \Delta(\epsilon) = (\gamma^{\pm}_n)^2 \frac{1}{d_n \pi} \tag{1.68}$$

This leads to the form of

$$\int_{-1}^{1} d\epsilon h(\epsilon) d^{\dagger} a_{\epsilon} = d^{\dagger} \sum_{n} [a_n \int^{+,n} h(\epsilon)\psi_n^{+} + b_n \int^{-,n} h(\epsilon)\psi_n^{-}] \tag{1.69}$$

$$= d^{\dagger} \sum_{n} [a_n \int^{+,n} h(\epsilon)\frac{1}{\sqrt{d_n}} + b_n \int^{-,n} h(\epsilon)\frac{1}{\sqrt{d_n}}] \tag{1.70}$$

$$= d^{\dagger} \sum_{n} [a_n h_n^{+}\frac{1}{\sqrt{d_n}} + b_n h_n^{-}\frac{1}{\sqrt{d_n}}] = \frac{1}{d_n\sqrt{\pi}} d^{\dagger} \sum_{n} [a_n \gamma_n^{+} + b_n \gamma_n^{-}] \tag{1.71}$$

Next we deal with the bath term:

$$\int_{-1}^{1} d\epsilon g(\epsilon) c_{\epsilon}^{\dagger} c_{\epsilon} = \sum_{np,mq} [a_{np}^{\dagger} a_{mq} \int^{+,n} d\epsilon g(\epsilon)\psi_{np}^{+}(\epsilon)\psi_{mq}(\epsilon) + b_{np}^{\dagger} b_{mq} \int^{-,n} d\epsilon g(\epsilon)\psi_{np}^{+}(\epsilon)\psi_{mq}^{-}(\epsilon)]$$

$$== \sum_{np} [a_{np}^{\dagger} a_{np} \int^{+,n} d\epsilon g(\epsilon) + b_{np}^{\dagger} b_{np} \int^{-,n} d\epsilon g(\epsilon)]\frac{1}{d_n} \tag{1.72}$$

We carry out the integration $\int^{\pm} xdx$

$$\int^{\pm} xdx\Delta(x) = \pi \int^{\pm} xdx \frac{dg^{-1}(x)}{dx} h^2[g^{-1}(x)] = \pi \int^{\pm} xdy h^2(y), y = g^{-1} \tag{1.73}$$

If we set $x = g(y)$, we have

$$\int^{\pm} xdy h^2(y) = \int^{\pm} g(y)dy h^2(y) \approx (h_n^{\pm})^2 \int^{\pm} g(\epsilon)d\epsilon \tag{1.74}$$

$$\int^{\pm} g(\epsilon)d\epsilon = \frac{1}{\pi(h_n^{\pm})^2} \int^{\pm} xdx\Delta(x) = d_n \frac{\int^{\pm} xdx\Delta(x)}{\int^{\pm} dx\Delta(x)} \tag{1.75}$$

In the lase equation, we have used the results for $(h_n^{\pm})^2$.

If we further define

$$(\gamma^{\pm})^2 = \int^{\pm} \Delta(x)dx, \xi_n^{\pm} = \frac{1}{(\gamma^{\pm})^2} \int^{\pm} x\Delta(x)dx \tag{1.76}$$

so

$$\int^{\pm} g(\epsilon)d\epsilon = d_n \frac{\int^{\pm} xdx\Delta(x)}{\int^{\pm} dx\Delta(x)} = d_n \xi_n^{\pm} \tag{1.77}$$

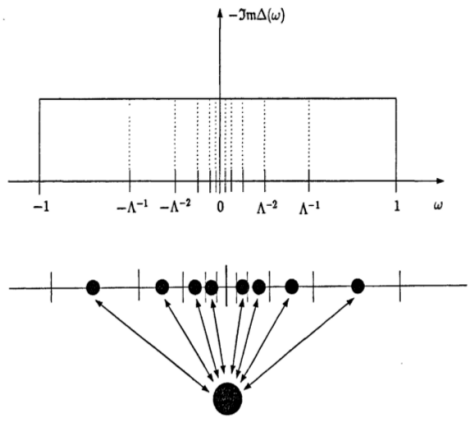

Figure 1.7: The logarithmic discretization of electron bath.

thus the bath term becomes

$$\int d\epsilon g(\epsilon) c_\epsilon^\dagger c_\epsilon = \sum_n \xi_n^+ a_n^\dagger a_n + \xi_n^- b_n^\dagger b_n \tag{1.78}$$

Finally, the original hamiltonian can be transformed to

$$H = E_d d^\dagger d + \sum_n [\xi_n^+ a_n^\dagger a_n + \xi_n^- b_n^\dagger b_n] + \frac{1}{\sqrt{\pi}} d^\dagger \sum_n [a_n \gamma_n^+ + b_n \gamma_n^-]/d_n + h.c. \tag{1.79}$$

Now this hamiltonian shows the coupling to all sites just as sketched in Fig. 1.7.

1.4.2 Mapping to semi-infinite chain

In the Hamiltonian for the Wilson chain, the impurity directly couples only to one conduction electron degree of freedom with operators f_0. With the definition

$$f_0 = \frac{1}{\sqrt{\eta_0}} \sum_n [\gamma_n^+ a_n + \gamma_n^- b_n] \tag{1.80}$$

$$\eta_0 = \sum_n (\gamma_n^+)^2 + (\gamma_n^-)^2 = \int_{-1}^{1} d\epsilon \Delta(\epsilon) \tag{1.81}$$

We have

$$H = E_d d^\dagger d + \sum_n [\xi_n^+ a_n^\dagger a_n + \xi_n^- b_n^\dagger b_n] + \sqrt{\frac{\eta_0}{\pi}} [f_0^\dagger d + d^\dagger f_0] \tag{1.82}$$

The operators f_0 represent the first site of the conduction electron part of the semi-infinite chain. These operators are of course not orthogonal to the operators a_n, b_n.

The desired semi-finite chain suitable for the NRG iteration is

$$H = E_d d^\dagger d + \sum_{n=0}^{N} \varepsilon_n f_n^\dagger f_n + \sum_{n=0}^{N-1} \tau_n (f_n^\dagger f_{n+1} + h.c.) + \sqrt{\frac{\eta_0}{\pi}} [f_0^\dagger d + d^\dagger f_0] \tag{1.83}$$

where τ_n is the hopping matrix element and ε_n is on-site energies, with the operators f_n corresponding to the nth site of the conduction electron part of the chain.

The Lanczos procedure needs to transform the all-coupled hamilton to the desired form. It should complete such a task: Using $\Delta(\epsilon)$ as input gives ε_n, τ_n.

The operator f_n and operators a_n, b_n are related via the orthogonal transformation

$$a_n = \sum_{m=0}^{\infty} u_{mn} f_m, b_n = \sum_{m=0}^{\infty} v_{mn} f_m, \tag{1.84}$$

$$f_n = \sum_{m=0} u_{nm} a_m + v_{nm} b_m \tag{1.85}$$

For the definition of f_0, we can read off the coefficient u_{0m}, v_{0m}

$$u_{0m} = \gamma_m^+ / \sqrt{\eta_0}, v_{0m} = \gamma_m^- / \sqrt{\eta_0} \tag{1.86}$$

1.4.3 Iterative diagonalization

The transformations described so far are necessary to map the problem onto a form for which an iterative renormalization group (RG) procedure can be defined. This is the point at which, finally, the RG character of the approach enters

The chain Hamiltonian can be viewed as a series of Hamiltonians $H_N (N = 0, 1, 2, ...,$ which

approaches H in the limit$N \to \infty$:

$$H = \lim_{N\to\infty} \Lambda^{-(N-1)/2} H_N \tag{1.87}$$

$$H_N = \Lambda^{(N-1)/2}[E_d d^\dagger d + \sum_{n=0}^{N} \varepsilon_n f_n^\dagger f_n + \sum_{n=0}^{N-1} \tau_n (f_n^\dagger f_{n+1} + h.c.) + \sqrt{\frac{\eta_0}{\pi}}[f_0^\dagger d + d^\dagger f_0]] \tag{1.88}$$

$$= \sqrt{\Lambda} H_{N-1} + \Lambda^{(N-1)/2}[\varepsilon_N f_N^\dagger f_N + \tau_N (f_N^\dagger f_{N-1} + h.c.)] \tag{1.89}$$

The starting point of the sequence of Hamiltonians is given by a two-site cluster formed by the impurity and the first conduction electron site. Note that in the special case of the siAm, one can also choose $H_{-1} = H_{imp}$ as the starting point (with a proper renaming of parameters and operators) since the hybridization term has the same structure as the hopping term between the conduction electron sites. The recursion relation can now be understood in terms of a renormalization group transformation R:

$$H_N = R(H_{N-1}) \tag{1.90}$$

In a standard RG transformation, the Hamiltonians are specified by a set of parameters K and the mapping R transforms the Hamiltonian $H(K)$ into another Hamiltonian of the same form, $H(K')$, with a new set of parameters K'. Such a representation does not exist, in general, for the H_N which are obtained in the course of the iterative diagonalization to be described below. Instead, we characterize H_N, and thereby also the RG flow, directly by the many-particle energies $E_N(r)$,

$$H_N |r_N\rangle_N = E_N(r) |r\rangle_N, r = 1, 2, ..., N_s \tag{1.91}$$

with the eigenstates $|r\rangle_N$ and N_s the dimension of H_N. This is particularly useful in the crossover regime between different fixed points, where a description in terms of an effective Hamiltonian with certain renormalized parameters is not possible. Only in the vicinity of the fixed points (except for certain quantum critical points) one can go back to an effective Hamiltonian description, as described below. Our primary aim now is to set up an iterative scheme for the diagonalization of H_N, in order to discuss the flow of the many-particle energies $E_N(r)$. Let us assume that, for a given N, the Hamiltonian H_N has already been diagonalized. We now construct a basis for H_{N+1}, as sketched in Fig. 1.8:

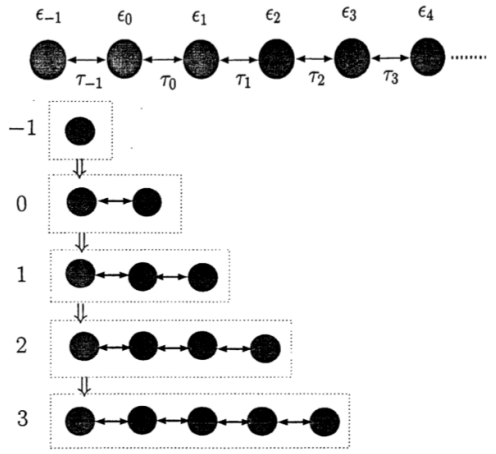

Figure 1.8: In each step of the iterative diagonalization scheme one site of the chain (with operators f_{N+1}) and on-site energy ε_{N+1}) is added to the Hamiltonian H_N. A basis $|r; s_{N+1}\rangle$ for the resulting Hamiltonian, H_{N+1}, is formed by the eigenstates of $|r\rangle$, and a basis of the added site, $|s_{(N+1)}\rangle$.

$$|r; s\rangle_{N+1} = |r\rangle_N \otimes |s(N+1)\rangle \tag{1.92}$$

The states $|r; s(N+1)\rangle$ are product states consisting of the eigenbasis of H_N and a suitable basis $s(N+1)$ for the added site (the new degree of freedom). From the new constructed basis we construct the Hamiltonian matrix for H_{N+1}:

$$H_{N+1}(rs, r's') =_{N+1} \langle r; s|H_{N+1}|r'; s'\rangle_{N+1} \tag{1.93}$$

Diagonalization of the matrix gives the new eigenenergies $E_{N+1}(w)$ and eigenstates $|w\rangle_{N+1}$ which are related to the basis $|r; s(N+1)$ via the unitary matrix U:

$$|w\rangle_{N+1} = \sum_{rs} U(w, rs)|r; s(N+1)\rangle \tag{1.94}$$

The following steps are illustrated in Fig. 1.9: In Fig. 1.9a we show the many-particle spectrum of H_N, that is the sequence of many-particle energies $E_N(r)$. Note that, for convenience, the ground-state energy has been set to zero. Figure b shows the overall scaling of the energies by the factor.

The increasing number of states is, of course, a problem for the numerical diagonalization; the dimension of H_{N+1} grows exponentially with N, even when we consider symmetries of the model

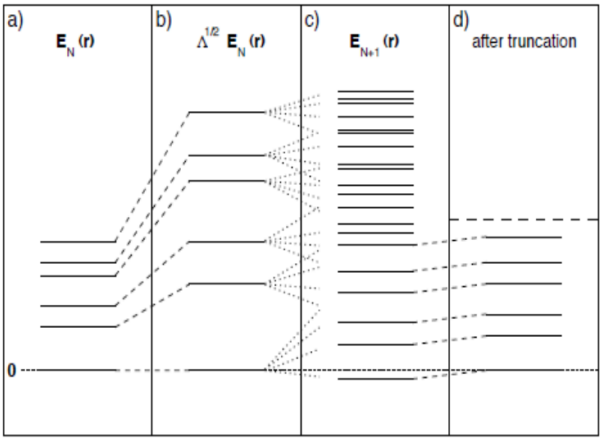

Figure 1.9: (a)Many-particle spectrum $E_N(r)$ of the Hamiltonian H_N with the ground-state energy set to zero. (b): The relation between successive Hamiltonians includes a scaling factor. (c) Many-particle spectrum $E_{N+1}(r)$ of H_{N+1}, calculated by diagonalizing the Hamiltonian matrix. (d) The same spectrum after truncation where only the N_s lowest-lying states are retained; the ground-state energy has again been set to zero..

so that the full matrix takes a block-diagonal form with smaller submatrices. This problem can be solved by a very simple truncation scheme: after diagonalization of the various submatrices of H_{N+1} one only keeps the Ns eigenstates with the lowest many-particle energies. In this way, the dimension of the Hilbert space is fixed to Ns and the computation time increases linearly with the length of the chain. Suitable values for the parameter Ns depend on the model; for the siAm, Ns of the order of a few hundred is sufficient to get converged results for the many-particle spectra, but the accurate calculation of static and dynamic quantities usually requires larger values of Ns.

Such an ad-hoc truncation scheme needs further explanations. First of all, there is no guarantee that this scheme will work in practical applications and its quality should be checked for each individual application. Important here is the observation that the neglect of the high-energy states does not spoil the low-energy spectrum in subsequent iterations this can be easily seen numerically by varying N_s. The influence of the high-energy on the low-energy states is small since the addition of a new site to the chain can be viewed as a perturbation of relative strength $\Lambda^{-1/2} < 1$. This perturbation is small for large values of Λ but for $\Lambda \to 1$ it is obvious that one has to keep more and more states to get reliable results. This also means that the accuracy of the NRG results is getting worse when Ns is kept fixed and Λ is reduced.

From this discussion we see that the success of the truncation scheme is intimately connected to the special structure of the chain Hamiltonian (that is $\tau_n \sim \Lambda^{-n/2}$) which in turn is due to

the logarithmic discretization of the original model.

1.4.4 Summary

For basically all NRG applications, one proceeds as follows: a) Division of the energy support of the bath spectral function into a set of logarithmic intervals.

b) Reduction of the continuous spectrum to a discrete set of states (logarithmic discretization).

c) Mapping of the discretized model onto a semiinfinite chain.

d) Iterative diagonalization of this chain.

e) Further analysis of the many-particle energies, matrix elements, etc., calculated during the iterative diagonalization. This yields information on fixed points, static and dynamic properties of the quantum impurity model.